Ceramics International 47 (2021) 1399–1406

Contents lists available at ScienceDirect

Ceramics International

journal homepage: www.elsevier.com/locate/ceramint

A novel IR-transparent Ho^{3+}:Y_2O_3–MgO nanocomposite ceramics for potential laser applications

N.A. Safronova [a], R.P. Yavetskiy [a,*], O.S. Kryzhanovska [a], M.V. Dobrotvorska [a], A.E. Balabanov [a], I.O. Vorona [a], A.V. Tolmachev [a], V.N. Baumer [b], I. Matolínová [c], D.Yu. Kosyanov [d], O. O. Shichalin [d,e], E.K. Papynov [d,e], S. Hau [f], C. Gheorghe [f]

[a] Institute for Single Crystals, NAS of Ukraine, 60 Nauky Avenue, Kharkiv, 61072, Ukraine
[b] SSI "Institute for Single Crystals", NAS of Ukraine, 60 Nauky Avenue, Kharkiv, 61072, Ukraine
[c] Charles University, Faculty of Mathematics and Physics, V Holešovičkách 2, Prague, 18000, Czech Republic
[d] Far Eastern Federal University, 8 Sukhanova Street, Vladivostok, 690950, Russian Federation
[e] Institute of Chemistry, Far-Eastern Branch, Russian Academy of Sciences, 159 100-let Vladivostoku Avenue, Vladivostok, 690022, Russian Federation
[f] National Institute for Laser, Plasma and Radiation Physics, ECS Laboratory, PO Box MG-36, 077125, Magurele, Bucharest, Romania

ARTICLE INFO

Keywords:
Transparent ceramics
Nanocomposite
Spark plasma sintering
Eye-safe lasers
Luminescence

ABSTRACT

The work is devoted to obtaining of transparent nanocomposite materials as low loss, highly thermally conductive materials for potential laser applications. We report Ho^{3+}:Y_2O_3–MgO nanocomposite ceramics with excellent mechanical and optical properties by combining glycine-nitrate process and spark plasma sintering. Morphology, structural-phase state, infrared transmittance and luminescence depending on the holmium concentration (0–12 at.%) were studied for the first time. It was found that optical transmittance reaches 75% @6000 nm for 3 at.% Ho^{3+}:Y_2O_3–MgO ceramics. The absorption cross-section at 1931 nm and the emission cross-section at 2118 nm were determined to be $\sigma_{abs} = 0.51 \times 10^{-20}$ cm^2 and $\sigma_{em} = 0.29 \times 10^{-20}$ cm^2, respectively. Based on the testing results of luminescent characteristics it was demonstrated that Ho^{3+}:Y_2O_3–MgO nanocomposite is a promising material for high-power eye-safe lasers operating in the 2 μm wavelength range.

1. Introduction

Lasers emitting in the mid-infrared (mid-IR) spectral range (2–6 μm) are of great interest for use in a wide variety of applications including industry, atmospheric sensing, LIDARs and medicine. General trend in creation of such lasers is a search for the most promising high thermal conductivity host materials. In particular, single crystalline MgO has a room temperature thermal conductivity from ~60 W m^{-1} K^{-1} to ~80 W m^{-1} K^{-1} [1], which is gigantic in comparison with that of the most used laser material YAG (~11 W m^{-1} K^{-1}) and should result in a desirable advance in laser power scalability. Recently, new transparent ceramics for solid-state lasers based on trivalent rare-earths (RE^{3+}) doped Al_2O_3 [2,3], MgO [1], and $MgAl_2O_4$ [4,5] have been actively explored. However, the fabrication of laser media based on RE-doped Al_2O_3, MgO, and $MgAl_2O_4$ encounters significant difficulties due to the low solubility limit of RE ions in host materials.

The key to solve the problem of low loss, highly thermally conductive transparent ceramics for potential laser applications may be the development of transparent nanocomposite materials. The advantages of transparent nanocomposites include high optical quality inherent to single crystals, higher thermal conductivity and mechanical properties compared to the constituent oxides. In order to produce transparent composite nanoceramics with controlled grain size low-agglomerated nanopowders with average particle size 10–50 nm as well as their consolidation in non-equilibrium conditions are required [6]. The basic strategy for the synthesis of composite nanoceramics is to control their structural-phase state at the nanoscale by using consolidation methods that suppress the diffusion mass transfer such as spark-plasma sintering (SPS), hot isostatic pressing (HIP), etc. The optical transparency of nanoceramics in the IR range of the spectrum occurs due to the low light scattering on defects and interphase boundaries with characteristic dimensions of several nm. Fabrication of composite nanoceramics involves the creation of a nanocomposite of two or more non-soluble components in the solid state. In this case, grain growth can be suppressed due to the

* Corresponding author. Institute for Single Crystals, NAS of Ukraine, 60 Nauky Ave., Kharkiv, 61072, Ukraine.
E-mail address: yavetskiy@isc.kharkov.ua (R.P. Yavetskiy).

https://doi.org/10.1016/j.ceramint.2020.08.263
Received 17 June 2020; Received in revised form 31 July 2020; Accepted 30 August 2020
Available online 2 September 2020

fact that the grains of each phase pin the boundary of the other phase [7–9]. At the same time, the requirement to ensure transparency of nanocomposite in a wide range of wavelengths requires the use of materials with a cubic structure and wide transparency windows. The optical transmission of composite nanoceramics will be realized for average grain sizes of less than 150–200 nm, whereby the contribution of light scattering at the interphase boundaries will be minimal.

Recently, fabrication of Y_2O_3–MgO transparent nanocomposite ceramics has been reported [10–12]. Moreover, Er^{3+}:Y_2O_3–MgO nanocomposite ceramics for mid-IR solid-state lasers have been designed [13–15]. In Y_2O_3–MgO material, RE^{3+} ions prefer to substitute Y^{3+} ions of the Y_2O_3 constituent, which is itself a promising laser host due to its high optical transparency in the wavelength range of 0.2–8 μm, high isomorphic capacity for the introduction of luminescent ions, low energy of phonons, low concentration quenching of luminescence, etc. Ho^{3+}:Y_2O_3 ceramics were actively studied as a promising material for mid-IR solid-state lasers emitting at ~2 μm, typically used in medical applications, remote sensing of atmospheric CO_2 and H_2O, laser ranging and time-resolved spectroscopy [16–20]. Resonantly pumped Ho-doped yttria is becoming more and more attractive to produce eye-safe lasers operating at wavelengths of 2–2.2 μm due to the inherently high efficiency and relatively simple thermal management [19]. Up to date, continuous-wave output power at 2117 nm has been generated with a slope efficiency of 55.6% using 0.5 at.% Ho^{3+}:Y_2O_3 ceramics [18]. Further power scaling could be, in principle, achieved with Ho^{3+}:Y_2O_3–MgO nanoceramics, since the thermal conductivity of composite lies between those of constituents: Y_2O_3–MgO – 18 W m^{-1} K^{-1}, Y_2O_3 – 13.6 W m^{-1} K^{-1}, MgO – 60–80 W m^{-1} K^{-1} at the room temperature [11]. However, to the best of our knowledge, there are no reports on preparation and properties of Ho^{3+}:Y_2O_3–MgO nanocomposite ceramics in the modern literature.

Recently, we have reported the fabrication of Y_2O_3–MgO composite ceramics by combining glycine-nitrate process (GNP) synthesis and SPS [21,22]. This work is devoted to the study of the obtaining features and optical properties of Ho^{3+}:Y_2O_3–MgO composite optical nanoceramics doped with different concentrations (0, 3, 6, and 12 at.%) of Ho^{3+} ions. The structural-phase state of Ho^{3+}:Y_2O_3–MgO nanocomposite ceramics obtained by SPS via glycine-nitrate processes, as well as their optical and luminescent properties have been investigated.

2. Experimental

Holmium-doped 50:50 vol% Y_2O_3–MgO (further denoted as Ho^{3+}:Y_2O_3–MgO) nanopowders were synthesized via the glycine-nitrate process according to Ref. [21]. Then, the obtained Ho^{3+}:Y_2O_3–MgO powders were loaded into a graphite die (inner diameter of 15 mm). Sintering was carried out using an SPS-515S apparatus (Dr. Sinter*LAB, Japan) at the temperature T = 1300 °C for 5 min and a pressure of 30 MPa. After that, the nanocomposite ceramics were mirror polished on both surfaces with different grade of the diamond slurries.

The microstructure of the obtained nanoceramics was studied by the filed-emission scanning electron microscopy (FE-SEM) and energy dispersion X-ray spectroscopy (EDX) using a Tescan Mira3 electron microscope. The average grain size of the ceramics was determined by using the linear intercept method. At least 300 Y_2O_3/MgO grains were analyzed for each measurement. The phase identification was performed by X-ray diffraction method (XRD) using a SIEMENS D-500 X-ray diffractometer ($Cu_{K\alpha}$-radiation, graphite monochromator). The mechanical properties of ceramics were investigated by the microhardness method based on deformation by concentrated load. The indentation was realized using a PMT-3 device with the standard tetrahedral indenter at the load 1 *N*, and the obtained indenter imprints were collected by means of a Zeiss Axioskop 40 A POL optical microscope. The optical properties of ceramics were studied using a Fourier-Transform Infrared (FTIR) spectrometer (Vertex-80, Bruker Optik GmbH, Germany) in the wavelength range of 1000–10000 nm. The absorption and emission spectra were recorded at 300 K with a setup consisting of a Jarell Ash monochromator, Ge photodiode and a Lock-in amplifier connected with a computer. A halogen lamp and a 350 W Xe–Hg lamp were used as excitation sources for the absorption and emission measurements, respectively. Laser grade polished samples with a thickness of 0.5 mm have been investigated.

3. Results and discussion

In order to minimize the optical scattering loss, a number of special requirements are put forward microstructure of composite material. The main one is the average grain size that should be significantly less than the wavelength of the incident light (~0.1 μm [12]). The difficulty in fulfilling this requirement is associated with the uncontrolled grain growth due to the recrystallization during sintering. An effective solution to stabilize the grain size of ceramics is to ensure a uniform distribution of the components of the Y_2O_3 and MgO mixture. Thus, the grain growth will be limited by the number of neighboring grains with similar composition. It is also known that any inhomogeneities at the phase boundary, whether pores or secondary phases, will reduce the transmittance of the material due to the high difference in the refractive indices of the phases. That is why the doping of the ceramics should be achieved without segregation of impurities at the grain boundaries and the formation of secondary phases. The structural and chemical homogeneity of Ho^{3+}:Y_2O_3–MgO composite ceramics depending on the doping concentration were studied using the FESEM method (Fig. 1). As can be observed, the ceramics are characterized by a high density and the absence of open pores, regardless of the holmium ions concentration. This can be attributed to the low agglomeration of the starting nanopowders and their high sinterability. All ceramics were characterized by a biphasic microstructure with a uniform grain distribution of both phases in the sample (according to mass contrast, dark grains are MgO phase, light grains are Y_2O_3). The average grain size of Y_2O_3 and MgO was about 200 and 190 nm, respectively, and no significant differences in the average grain size of composite depending on holmium concentration were found. This result agrees with that obtained for Er^{3+}:Y_2O_3–MgO system [15], and could be connected with the fact that trivalent dopants should have little effect on grain boundary mobility of yttria [23].

The detailed study of the ceramic samples on the nanoscale using FESEM method shows that all samples contain a few inclusions of an impurity phase, which are localized both at grain boundaries and triple junctions (Fig. 1b). The typical size of the inclusions lies within 1–15 nm range, which hampers the reliable establishment of their elemental composition. It was not possible to connect the number of inclusions with the holmium content due to the random localization of the secondary phase in ceramics. Based on the mass contrast, the inclusions represent a holmium-containing phase, namely, holmium oxide or carbide (Fig. 1b). The Y_2O_3–Ho_2O_3 phase diagram is unknown; according to Ref. [25] one should expect it to a full mutual solubility of holmium oxide in yttria. Thus, most probably, the precipitate phase is holmium carbide. In fact, the formation of holmium carbide could relate to the peculiarities of the powder processing and consolidation in graphite tooling. It should be noted that no inclusions at the grain boundaries were observed in undoped Y_2O_3–MgO composite ceramics [22].

EDX analysis confirms the uniform distribution of the main components of ceramics (yttrium and magnesium) within ceramic's volume (Fig. 2a). A homogenous phase distribution allows stabilizing the grain size of the nanocomposite, since each grain is an obstacle to grain growth of the other phase [9,22,25]. According to the EDX analysis, the ratio of the components of the composite ceramics is stoichiometric. For example, for the 3 at.% Ho^{3+}:Y_2O_3–MgO ceramics, the mass concentration of elements are: c (Mg) = 28 ± 3 wt% (24.8%), c(Y) = 41 ± 3 wt % (44.0%), c (Ho) = 1.7 ± 0.2 wt% (2.5%). The small discrepancy between the measured and theoretical values given in brackets may be due to the overlapping of Mg and Ho lines in the energy dispersion spectra.

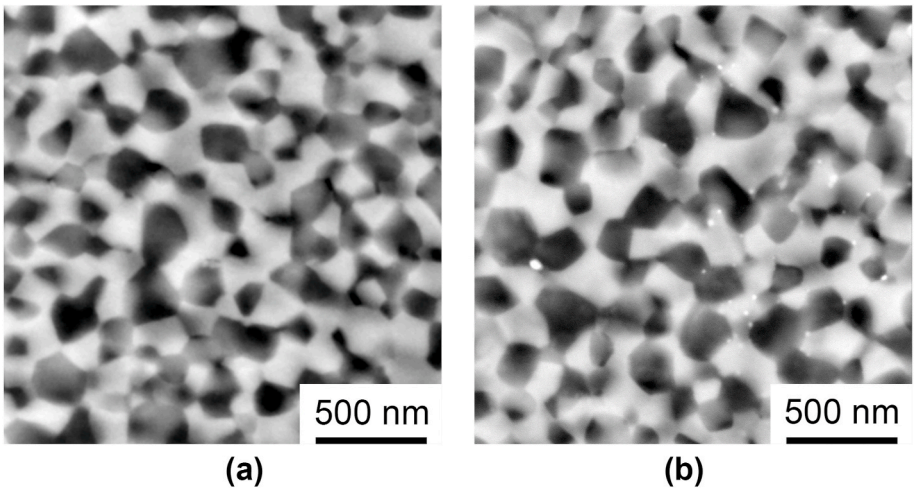

Fig. 1. FESEM of 3 at.% Ho^{3+}:Y_2O_3–MgO composite ceramics: general view (a), and area with secondary phase (b).

The intensity of the characteristic lines of holmium increases in the 3 to 12 at.% concentration range of Ho^{3+} ions (Fig. 2b). No other elements were detected within the sensitivity of the EDX measurements.

The solubility of holmium ions in Y_2O_3–MgO nanocomposite is of great importance, since doping of only yttria constituent will provide required functional response. While preferred solubility of holmium ions in yttria matrix is expected [24], formation of Ho^{3+}:MgO solid solution cannot be completely excluded taking into account the results reported in Ref. [1] and non-equilibrium synthesis conditions. The effect of Ho^{3+} doping on lattice parameters of Y_2O_3–MgO ceramics was studied by XRD method (Fig. 3). A typical diffraction pattern of 6 at.% Ho^{3+}:Y_2O_3–MgO is given in Fig. 3a. All the samples represent a mixture of cubic yttrium oxide (space group Ia3, JCPDS No. 41–1105) and cubic magnesium oxide (space group *Fm3m*, JCPDS No. 45–0946). The content of the main phases is Y_2O_3 – 57.7 wt%, MgO – 42.3 wt%, which agrees well with the stoichiometric values for the 50:50 vol ratio (Y_2O_3 – 58.2 wt%, MgO – 41.8 wt%). No impurity phases were detected within the method sensitivity. This suggests that the amount of the impurity holmium-containing phase revealed by FESEM is less than 1 wt% (Fig. 1b).

The lattice parameter *a* of yttrium oxide negligibly increases from 10.58903 (10)Å to 10.59105 (9)Å with the growth of Ho^{3+} ions concentration in the 3–12 at.% range (Fig. 3b). This is due to the partial replacement of Y^{3+} ions by Ho^{3+} ions with a slightly larger ionic radius (104 pm and 104.1 pm, correspondingly) [26]. The linear dependence of the lattice parameter on the holmium concentration indicates the formation of $(Y_{1-x}Ho_x)_2O_3$ substitutional solid solutions in the range of studied concentrations, according to the Vegard's rule. The lattice parameter of magnesium oxide decreases while the concentration of Ho^{3+} ions increases. Such behavior suggests that Ho^{3+} ions do not substitute Mg^{2+} ions (ionic radius of Mg^{2+} = 86 pm) in the MgO structure. The shrinkage of MgO lattice is connected with the loss of some oxygen in the reducing environment (vacuum) at high temperatures [27].

Microhardness is known to be one of the main parameters determining stability to thermal shock, which is particularly important for lasers, IR-windows and domes [11]. Y_2O_3–MgO composite is known to have improved mechanical hardness compared to Y_2O_3 and MgO single-phase ceramics [11]. The mechanical properties of Ho^{3+}:Y_2O_3–MgO sintered ceramics have been analyzed by the microindentation test. The highest Vickers hardness of 10.7 MPa was achieved with 12 at.% Ho^{3+}:Y_2O_3–MgO sample. This value is comparable to that of undoped Y_2O_3–MgO nanocomposite [22] and slightly exceeds the hardness of Er^{3+}:Y_2O_3–MgO ceramics (~10 MPa regardless of the doping concentration) [15]. This fact is unexpected, since Er^{3+}:Y_2O_3–MgO ceramics are characterized by much smaller grains size than those obtained in our experiments, of about 70 nm [15]. The increase in the hardness of Ho^{3+}:Y_2O_3–MgO most likely occurs due to the accumulation of dislocations during the preparation of the composites by the SPS method, which is considered to be more nonequilibrium in comparison with hot pressing used by Ma et al. [15].

The optical properties of transparent ceramics greatly depend on their structural and compositional homogeneity. For example, to achieve excellent transparency the pore concentration must be below 10^{-3} vol%, and the absence of secondary phases and clean grain boundaries with a typical width of about 1 nm are required. The IR transmittance spectra of Ho^{3+}:Y_2O_3–MgO composite ceramics are shown in Fig. 4a. It is worth noting that the optical properties of Ho^{3+}:Y_2O_3–MgO nanocomposite are limited in the visible range due to the light scattering at the grain boundaries of Y_2O_3 and MgO phases having different refractive indexes. The measured transmittance is slightly lower than the theoretical value due to scattering by the secondary phase, as well as by the nano- and micropores not revealed by the FESEM method. Wide peaks at 2800–4000 nm and 7000 nm detected in the spectra of sintered ceramics were attributed to the absorption of hydroxyl and carboxylate groups, respectively [22]. The highest in-line transmittance of 75%@6000 nm was obtained for ceramics doped with 3 at.% of Ho^{3+} ions (Fig. 4a), which is 5% higher compared to undoped Y_2O_3–MgO [22]. Since the Ho–O bond is weaker than the Y–O bond (bond dissociation energy D_{298} = 606 kJ mol^{-1} and D_{298} = 714 kJ mol^{-1}, correspondingly [28]), the ionicity degree of Ho–O bonds is smaller compared to that of Y–O. Therefore, the substitution of a certain amount of Y^{3+} ions by Ho^{3+} ions leads to a decrease in the electron density of oxygen atoms around holmium ions [29]. This will enhance diffusion of yttrium ions, increase sinterability that results in better optical transmittance of doped ceramics compared to undoped one. Further, an increase in the activator concentration up to 12 at.% results in a degradation of the optical transmittance down to 55%. Apparently, the concentration of holmium-containing inclusions located at grain boundaries vary for different Ho^{3+} content, leading to transmittance decrease (Fig. 4a). Further optimization of processing conditions is underway in order to increase in-line transmittance of nanocomposite. There are several ways to improve transmittance in both NIR and even visible wavelength range. The first one is more precise control of the particle size of starting nanopowders during glycine-nitrate process. Assuming that the grain growth factor remains the same for SPS of nanopowders having different particle size, utilization of powders consisting from smaller particles (20–40 nm) will result in ceramics with lower average grain size. This will allow to increase optical transmittance of nanocomposite due to lower scattering at interphase grain boundaries. The second way is using

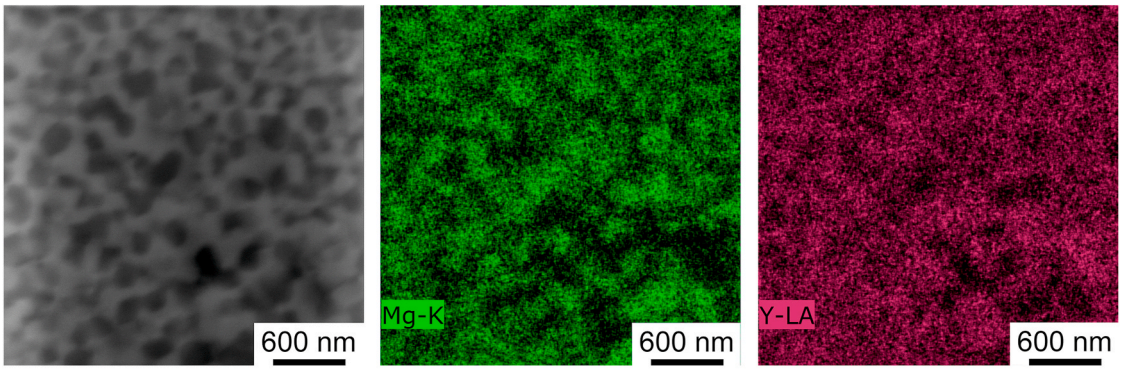

(a)

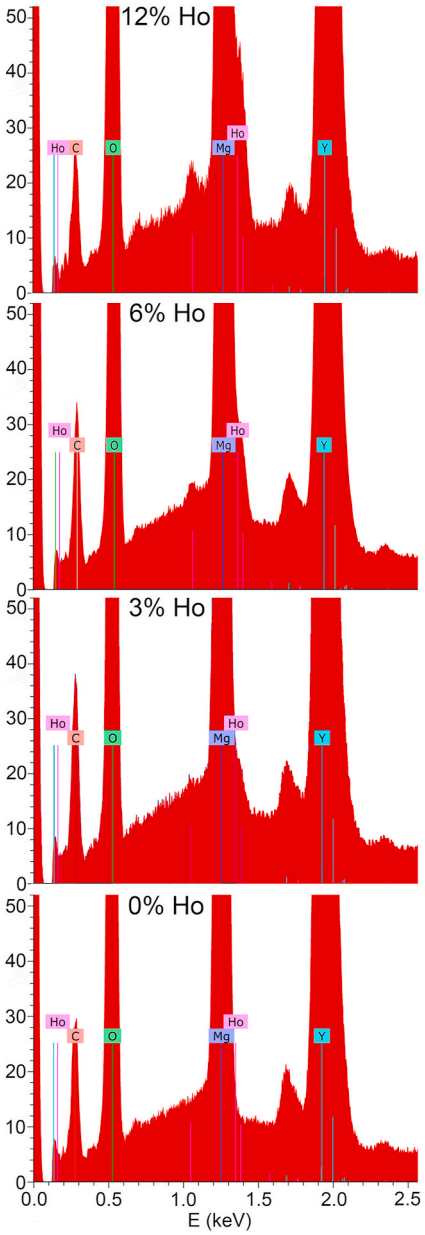

(b)

Fig. 2. Elemental mapping of Mg and Y in 6 at.% Ho^{3+}:Y_2O_3–MgO ceramics (a); EDX spectra of Ho^{3+}:Y_2O_3–MgO ceramics doped by 0, 3, 6, and 12 at.% of Ho^{3+} ions (b).

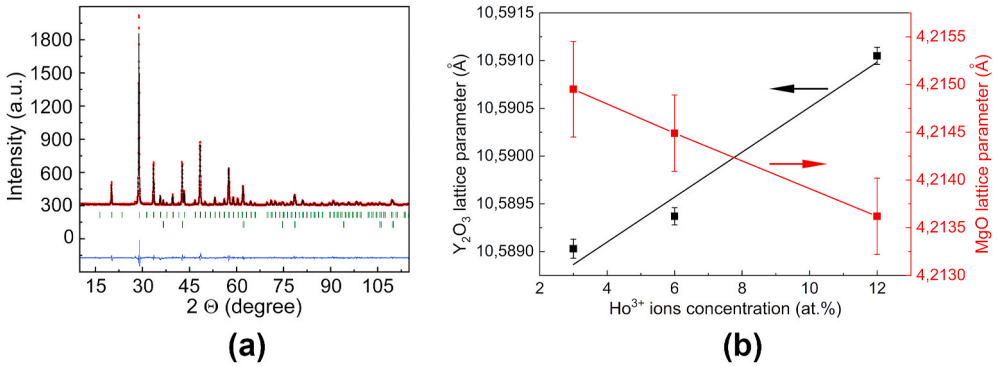

Fig. 3. X-ray diffraction pattern of 6 at.% Ho^{3+}:Y_2O_3–MgO composite ceramic (a); lattice parameters of Y_2O_3 and MgO vs. concentration of Ho^{3+} ions (b).

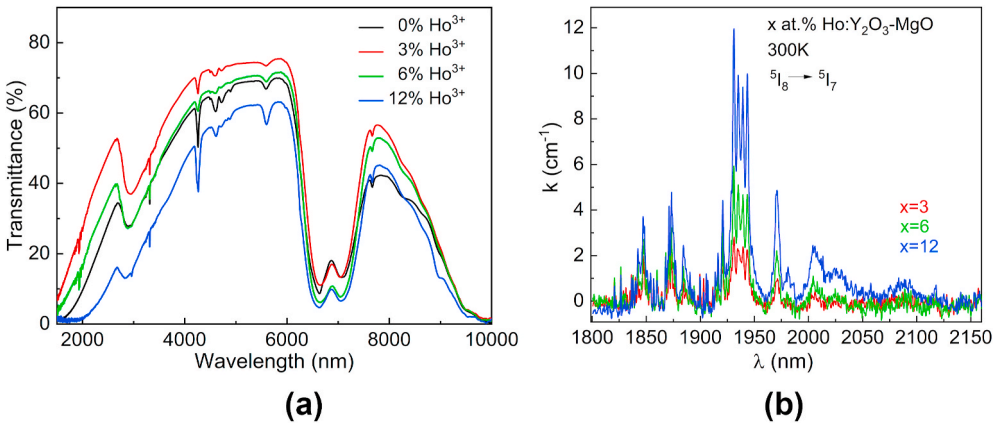

Fig. 4. IR transmittance of *x* at.% Ho-doped in Y_2O_3–MgO, *x*=(0, 3, 6, 12), nanocomposites (the thickness of the samples is 1 mm) (a); the absorption spectra of *x* at. % Ho-doped Y_2O_3–MgO nanocomposites corresponding to the Ho^{3+} $^5I_8 \rightarrow {}^5I_7$ transitions (b).

of sinter-HIP approach, which permits to suppress the diffusion processes significantly and keep the grain size at the 0.1 μm scale. Using this concept, authors [15] achieved in-line transmittance of Er:Y_2O_3–MgO composite as high as 80%@2100 nm while retaining the average grain size in the 110–120 nm range.

The room temperature absorption spectra of *x* at.% Ho-doped Y_2O_3–MgO nanocomposites, where *x*=(3, 6, 12), corresponding to the $^5I_8 \rightarrow {}^5I_7$ transitions of Ho^{3+} ions, were measured in the 1800–2000 nm wavelength range (Fig. 4b). It can be observed that the absorption lines are narrow, and the peak positions do not vary with *x* (Ho^{3+} content), but the absorption coefficients scale linearly with *x*. Based on the measured absorption coefficients, the absorption cross-sections values were determined using the effective dopant ion number density of Ho^{3+} ions that contribute to the electric dipole transitions observed, attributed to Ho^{3+} ions located in Y sites with C_2 symmetry (3/4 from the Ho^{3+} ions content) in the Y_2O_3 lattice [30]. The effective dopant ion number densities were calculated to be $N_{eff} = 6.04 \times 10^{20}$ cm^{-3}, 12.09×10^{20} cm^{-3}, and 24.18×10^{20} cm^{-3}, for 3 at.%, 6. at%, and 12 at.%, respectively, Ho-doped Y_2O_3–MgO nanocomposites. Thus, the most intense peak of the $^5I_8 \rightarrow {}^5I_7$ transitions is situated at 1931 nm and has an absorption cross-section $\sigma_{abs} = 0.51 \times 10^{-20}$ cm^2, which is about half of to the value obtained for Ho:Y_2O_3 ceramic ($\sigma_{abs} = 1 \times 10^{-20}$ cm^2 at 1930 nm wavelength) [16].

The room temperature emission spectra of *x* at.% Ho-doped Y_2O_3–MgO nanocomposites under Xe–Hg (300 W) lamp excitation were also recorded. The luminescence spectra reveal multiple and intense emission bands of Ho^{3+} ions in the visible (Fig. 5a) and infrared domains (Fig. 5b). In the visible range (Fig. 5a), the emission spectra consist of an intense group of lines in the wavelength range of 535–565 nm, which can be attributed to the electric-dipole transitions of Ho^{3+} ions from the $^5S_2$, $^5F_4$ thermalized levels to the $^5I_8$ ground state. The group of lines at ~660 nm, attributed to $^5F_5 \rightarrow {}^5I_8$ transitions of Ho^{3+} ion, have a much lower intensity. The positions of the main group of lines are similar to those observed in the luminescence spectra of Ho^{3+}:Y_2O_3 ceramics, films, and nanopowders [31–33]. As can be observed, in the visible domain the luminescence intensity of Ho^{3+}:Y_2O_3–MgO composite ceramics decreases with the increasing of holmium ions concentration in the range 3–12 at.%. It should be noted that no shifting or broadening of the emission peaks is observed for the samples, which indicates that the dopant concentration does not induce radiation trapping effects or collateral emission bands.

Fig. 5b shows the infrared emission spectra around ~760 nm, corresponding to the $^5S_2$, $^5F_4 \rightarrow {}^5I_7$ transitions with low-intensity lines, and around ~1210 nm corresponding to the $^5I_6 \rightarrow {}^5I_8$ transitions with much higher intensity lines, indicating a standard picture of Ho^{3+} ions luminescence. The emission spectra were found to be in a good agreement with previous reports on Ho^{3+}:Y_2O_3 ceramics [32,34]. The emission cross-section at 1200 nm was calculated by Füchtbauer-Ladenburg (FL) formula [35], and the obtained value is $\sigma_{em} = 2.3 \times 10^{-21}$ cm^2, which is slightly higher than half of the value obtained for Ho:Y_2O_3 crystal ($\sigma_{abs} = 4.1 \times 10^{-21}$ cm^2 at 1216 nm) [36]. It can be observed that the intensity of the emission lines around ~1210 nm increases with the increasing holmium concentration in the range of 3–6 at.%, and decrease for 12 at.% indicating a significant deterioration of the luminescence intensity, most probably due to the luminescence quenching.

The most important lasing channel of Ho^{3+} in the yttria matrix lies at ~2.12 μm being attributed to the $^5I_7 \rightarrow {}^5I_8$ transitions with a significant magnetic dipole contribution. Therefore, the study of the luminescent properties of Ho-doped composite ceramics in the NIR spectral range is a very important task. The room temperature luminescence spectra

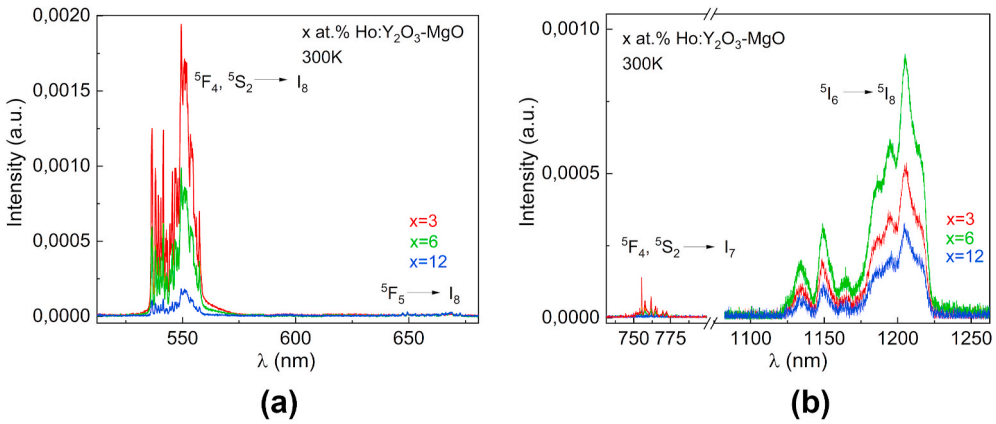

Fig. 5. Room temperature luminescence spectra of *x* at.% Ho-doped in Y_2O_3–MgO, *x*=(3, 6, 12), nanocomposites in visible (a) and infrared (b) domains.

corresponding to the $^5I_7 \rightarrow {}^5I_8$ transitions of Ho^{3+} ions doped in Y_2O_3–MgO nanocomposites are shown in Fig. 6a. The spectra exhibit intense emission bands of Ho^{3+} ions in the 1900–2150 nm wavelength range similar to those obtained for Ho^{3+}:Y_2O_3 ceramics [16].

The emission cross-section corresponding to the $^5I_7 \rightarrow {}^5I_8$ transitions (Fig. 6b) was also calculated by Füchtbauer-Ladenburg (FL) formula [35], and the obtained values are $\sigma_{em} = 0.57 \times 10^{-20}$ cm^2 at 2000 nm, $\sigma_{em} = 0.35 \times 10^{-20}$ cm^2 at 2088 nm, and $\sigma_{em} = 0.29 \times 10^{-20}$ cm^2 at 2118 nm, for all the samples. The obtained emission cross-section values around 2110 nm are close to those previously reported for 0.4 at.% Ho:Y_2O_3 crystal ($\sigma_{em} = 0.4 \times 10^{-20}$ cm^2 at 2111 nm) [37], 0.92 at.% Ho:Y_2O_3 crystal ($\sigma_{em} = 0.54 \times 10^{-20}$ cm^2 at 2116 nm) [36], and 1 at.% Ho:Y_2O_3 transparent ceramics ($\sigma_{em} = 0.45 \times 10^{-20}$ cm^2 at 2119 nm) [16], proving that Ho^{3+}:Y_2O_3–MgO nanocomposite could be a promising material for high-power eye-safe lasers operating at wavelengths ~2 μm.

As in the case of the emission spectra around 1200 nm, the intensities of the emission lines corresponding to the $^5I_7 \rightarrow {}^5I_8$ transitions increases with the increasing of holmium concentration in the range of 3–6 at.%. For 12 at.%, the emission intensity decrease due to the concentration quenching. The evolution of the emission intensities of these two $^5I_6 \rightarrow {}^5I_8$ and $^5I_7 \rightarrow {}^5I_8$ transitions can be explained by the existence of many and very efficient cross-relaxation processes. In general, the radiative lifetimes of the $^5I_6$ and $^5I_7$ manifolds of Ho^{3+} ions are very long, and therefore these manifolds act as energy reservoirs for cross-relaxation and excited-state absorption (ESA) processes [38]. In the case of Ho^{3+}:Y_2O_3 nanocrystals, these radiative lifetimes were found to be 6.8 ms and 12.3 ms, respectively [39].

The nonradiative energy transfer via dipole-dipole interaction between holmium ions excited to $^5F_4$, $^5S_2$ levels and unexcited, leads to the relaxation of the first ion and the excitation of the second, resulting thus in the transition of both ions on the $^5I_6$ and $^5I_7$ levels. Since the luminescence in the 535–565 nm spectral range is caused by the $^5F_4$, $^5S_2 \rightarrow {}^5I_8$ transitions, it is easy to see that the cross-relaxation processes will lead to a decrease in the number of photons emitted in the visible range and to an increase in the near IR domain. For example, different cross-relaxation processes involved in the depopulation of the $^5S_2$ manifold, such as ($^5S_2$, $^5I_7$)–($^5I_8$, $^5I_4$), ($^5F_3$, $^5F_5$)–($^5I_8$, $^5I_7$), ($^5S_2$, $^5I_7$)–($^5I_8$, $^5I_7$, $^5I_6$), and ($^5S_2$, $^5I_7$)–($^5F_5$, $^5I_6$), contribute to the population of $^5I_6$ and $^5I_7$ levels [38]. Furthermore, the probability of cross-relaxation is inversely proportional to the sixth power of the distance between the Ho^{3+} ions; thus, it will increase with increasing doping concentration [40].

4. Conclusions

50:50 vol% 3, 6, and 12 at.% Ho^{3+}:Y_2O_3–MgO nanocomposite ceramics were prepared by means of GNP and SPS techniques. The obtained ceramics are characterized by a biphasic structure with a uniform grain distribution of both phases in the sample, which allow effectively stabilize the average grain size of ceramics of about 200 nm. Holmium-containing secondary phases with dimension of 1–15 nm were revealed at the grain boundaries of nanocomposite due to the sintering features of ceramics by the SPS in graphite tooling. XRD shows that holmium ions enter only Y_2O_3 structure with the formation of $(Y_{1-x}Ho_x)_2O_3$ substitutional solid solutions in the whole concentration range of Ho^{3+} ions studied. The maximum value of Vickers hardness of 10.7 GPa was achieved for 12% Ho^{3+}:Y_2O_3–MgO ceramics. The highest in-line transmittance of 75%@6000 nm was obtained for ceramics doped with 3 at.% of Ho^{3+} ions, which is 5% higher compared to undoped Y_2O_3–MgO. This fact is connected with smaller ionicity degree of Ho–O bonds compared to that of Y–O, leading to enhanced diffusion in yttrium sublattice.

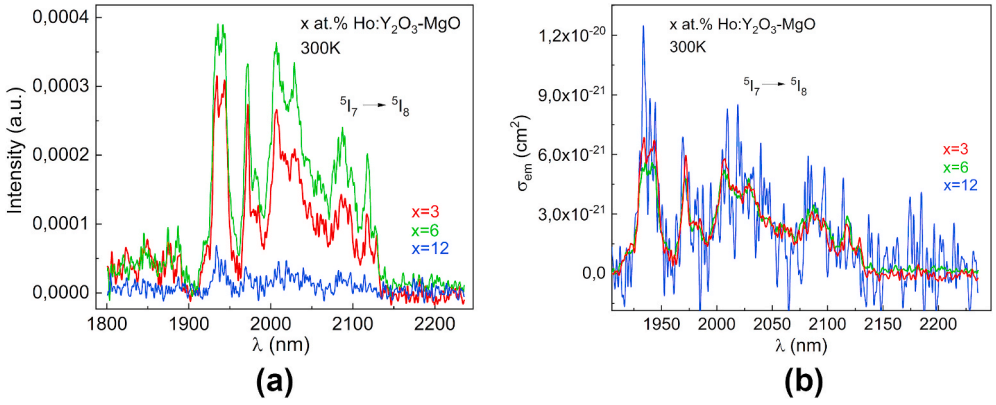

Fig. 6. Room temperature luminescence spectra (a) and emission cross-sections (b) corresponding to the $^5I_7 \rightarrow {}^5I_8$ transitions of *x* at.% Ho-doped in Y_2O_3–MgO, *x*=(3, 6, 12), nanocomposites.

All nanocomposite ceramics show dominant luminescence in the green and infrared domains, as well as a weak emission in the red domain. The 6% Ho^{3+}:Y_2O_3–MgO nanocomposite demonstrates the strongest emission intensity in the 1925–1975 nm wavelength range. It has been shown that increase of holmium concentration decreases the luminescence intensity at 550 nm ($^5F_4$, $^5S_2 \rightarrow {}^5I_8$) and increases those at 1200 nm ($^5I_6 \rightarrow {}^5I_8$) and 2000 nm ($^5I_7 \rightarrow {}^5I_8$) due to the cross-relaxation processes. The absorption cross-section at 1931 nm and the emission cross-section at 2118 nm were determined to be $\sigma_{abs} = 0.51 \times 10^{-20}$ cm^2 and $\sigma_{em} = 0.29 \times 10^{-20}$ cm^2, respectively, proving that Ho^{3+}:Y_2O_3–MgO nanocomposite could be a promising material for high-power eye-safe lasers operating at wavelengths ~2 μm.

Declaration of competing interest

The authors declare that they have no known competing financial interests or personal relationships that could have appeared to influence the work reported in this paper.

Acknowledgements

This work was supported by the National Academy of Sciences of Ukraine by the budget program "Support for the development of priority areas of scientific research" (KPKVK 6541230). The authors acknowledge the CERIC-ERIC Consortium for the access to FESEM experimental facility and financial support (proposal number 20192029). The authors are grateful to Dr. L. Gheorghe, Dr. E.F. Dolzhenkova and Dr. A.A. Kuchmizhak for their help in characterization of the ceramic samples.

References

[1] T. Sanamyan, C. Cooper, G. Gilde, A.C. Sutorik, M. Dubinskii, Fabrication and spectroscopic properties of transparent Nd^{3+}:MgO and Er^{3+}:MgO ceramics, Laser Phys. Lett. 11 (2014), 065801, https://doi.org/10.1088/1612-2011/11/6/065801.

[2] K. Drdlíková, R. Klement, D. Drdlík, T. Spusta, D. Galusek, K. Maca, Luminescent Er^{3+} doped transparent alumina ceramics, J. Eur. Ceram. Soc. 37 (2017) 2695–2703, https://doi.org/10.1016/j.jeurceramsoc.2017.02.017.

[3] E.H. Penilla, L.F. Devia-Cruz, M.A. Duarte, C.L. Hardin, Y. Kodera, J.E. Garay, Gain in polycrystalline Nd-doped alumina: leveraging length scales to create a new class of high-energy, short pulse, tunable laser materials, Light Sci. Appl. 7 (2018) 33, https://doi.org/10.1038/s41377-018-0023-z.

[4] R. Boulesteix, A. Maître, K. Lemański, P.J. Dereń, Structural and spectroscopic properties of $MgAl_2O_4$:Nd^{3+} transparent ceramics fabricated by using two-step spark plasma sintering, J. Alloys Compd. 722 (2017) 358–364, https://doi.org/10.1016/j.jallcom.2017.06.101.

[5] S.S. Balabanov, A.V. Belyaev, E.M. Gavrishchuk, I.B. Mukhin, A.V. Novikova, O. V. Palashov, D.A. Permin, I.L. Snetkov, Fabrication and measurement of optical and spectral properties of the transparent Yb:$MgAl_2O_4$ ceramics, Opt. Mater. 71 (2017) 17–22, https://doi.org/10.1016/j.optmat.2016.10.033.

[6] G.L. Messing, A.J. Stevenson, Toward pore-free ceramics, Science 322 (2008) 383–384, https://doi.org/10.1126/science.1160903.

[7] Jiwen Wang, Dianying Chen, E.H. Jordan, M. Gell, Infrared-transparent Y_2O_3–MgO nanocomposites using sol–gel combustion synthesized powder, J. Am. Ceram. Soc. 93 (2010) 3535–3538, https://doi.org/10.1111/j.1551-2916.2010.04071.x.

[8] Shengquan Xu, Li Jiang, Li Chaoyu, Yubai Pan, Jingkun Guo, Infrared-transparent Y_2O_3–MgO nanocomposites fabricated by the glucose sol–gel combustion and hot-pressing technique, J. Am. Ceram. Soc. 98 (2015) 2796–2802, https://doi.org/10.1111/jace.13681.

[9] Tao Dong, A. Jiang, K. Mukherjee, Spark plasma sintering of an infrared-transparent Y_2O_3–MgO nanocomposite, J. Am. Ceram. Soc. 93 (2010) 769–773, https://doi.org/10.1111/j.1551-2916.2009.03444.x.

[10] B.H. Kear, R. Sadangi, V. Shukla, T. Stefanik, R. Gentilman, Submicron-grained transparent yttria composites, Proc. SPIE 5786 (2005) 227–233, https://doi.org/10.1117/12.602333.

[11] D.C. Harris, L.R. Cambrea, L.F. Johnson, R.T. Seaver, M. Baronowski, R. Gentilman, C.S. Nordahl, T. Gattuso, S. Silberstein, P. Rogan, T. Hartnett, B. Zelinski, W. Sunne, E. Fest, W.H. Poisl, C.B. Willingham, G. Turri, C. Warren, M. Bass, D. E. Zelmon, S.M. Goodrich, Properties of an infrared-transparent MgO:Y_2O_3 nanocomposite, J. Am. Ceram. Soc. 96 (2013) 3828–3835, https://doi.org/10.1111/jace.12589.

[12] H.J. Ma, W.K. Jung, C. Baek, D.K. Kim, Influence of microstructure control on optical and mechanical properties of infrared transparent Y_2O_3-MgO nanocomposite, J. Eur. Ceram. Soc. 37 (2017) 4902–4911, https://doi.org/10.1016/j.jeurceramsoc.2017.05.049.

[13] V.L. Blair, Z.D. Fleischman, L.D. Merkle, N. Ku, C.A. Moorehead, Co-precipitation of rare-earth-doped Y_2O_3 and MgO nanocomposites for mid-infrared solid-state lasers, Appl. Optic. 56 (2017) B154–B158, https://doi.org/10.1364/AO.56.00B154.

[14] Z.D. Fleischman, V.L. Blair, N. Ku, L.D. Merkle, Dual-phase Er:Y_2O_3/MgO nanocomposites for mid-infrared solid-state lasers, Proc. SPIE (2018), 106370Z, https://doi.org/10.1117/12.2311470.

[15] Ho Jin Ma, Jung Wook Ki, Youngtae Park, Kim Do Kyung, A novel approach of an infrared transparent Er:Y_2O_3–MgO nanocomposite for eye-safe laser ceramics, J. Mater. Chem. C 6 (2018) 11096–11103, https://doi.org/10.1039/C7TC05991D.

[16] G.A. Newburgh, A. Word-Daniels, A. Michael, L.D. Merkle, Akio Ikesue, M. Dubinskii, Resonantly diode-pumped Ho^{3+}:Y_2O_3 ceramic 2.1 μm laser, Optic Express 19 (2011) 3604–3611, https://doi.org/10.1364/OE.19.003604.

[17] Yongguang Zhao, Jun Wang, Weichao Yao, Zhenhua Shao, Chongfeng Shen, Danlei Yin, Ying Wang, Peng Liu, Wei Zhou, Dingyuan Tang, Deyuan Shen, High-power Ho-doped sesquioxide ceramic laser in-band pumped by a Tm-doped all-fiber MOPA, IEEE Photonics. J 10 (2018), 1502107, https://doi.org/10.1109/jphot.2018.2820328.

[18] Fei Wang, Jinwen Tang, Enhao Li, Chongfeng Shen, Jun Wang, Dingyuan Tang, Deyuan Shen, Ho3+:Y2O3 ceramic laser generated over 113 W of output power at 2117 nm, Opt. Lett. 44 (2019) 5933–5936, https://doi.org/10.1364/OL.44.005933.

[19] Enhao Li, Jinwen Tang, Yajie Shen, Fei Wang, Jun Wang, Dingyuan Tang, Deyuan Shen, High peak power acousto-optically Q-switched Ho:Y_2O_3 ceramic laser at 2117 nm, IEEE Photon. Technol. Lett. 32 (2020) 492–495, https://doi.org/10.1109/LPT.2020.2981642.

[20] I.L. Snetkov, V.V. Balashov, Thermo-optical properties of Ho:Y_2O_3 ceramics, Opt. Mater. 100 (2020), 109617, https://doi.org/10.1016/j.optmat.2019.109617.

[21] O.S. Kryzhanovska, N.A. Safronova, A.E. Balabanov, R.P. Yavetskiy, M. V. Dobrotvorskaya, Li Jiang, S. Petrushenko, A.V. Tolmachev, N.A. Matveevskaya, E.N. Shulichenko, V.Y. Mayorov, D.S. Sofronov, Y_2O_3–MgO highly-sinterable nanopowders for transparent composite ceramics, Met. Funct. Mater. 26 (2019) 829–837, https://doi.org/10.15407/fm26.04.829.

[22] N.A. Safronova, O.S. Kryzhanovska, M.V. Dobrotvorska, A.E. Balabanov, A. V. Tolmachev, R.P. Yavetskiy, S.V. Parkhomenko, R. Brodskii, V.N. Baumer, D. Yu. Kosyanov, O.O. Shichalin, E.K. Papynov, Li Jiang, Influence of sintering temperature on structural and optical properties of Y_2O_3–MgO composite SPS ceramics, Ceram. Int. 46 (2020) 6537–6543, https://doi.org/10.1016/j.ceramint.2019.11.137.

[23] Pei-Lin Chen, I-Wei Chen, Grain boundary mobility in Y_2O_3: defect mechanism and dopant effects, J. Am. Ceram. Soc. 79 (1996) 1801–1809, https://doi.org/10.1111/j.1151-2916.1996.tb07998.x.

[24] E.R. Andrievskaya, Phase equilibria in the refractory oxide systems of zirconia, hafnia and yttria with rare-earth oxides, J. Eur. Ceram. Soc. 28 (2008) 2363–2368, https://doi.org/10.1016/j.jeurceramsoc.2008.01.009.

[25] Shengquan Xu, Li Jiang, Chaoyu Li, Yubai Pan, Jingkun Guo, Infrared-transparent Y_2O_3–MgO nanocomposites fabricated by the glucose sol–gel combustion and hot-pressing technique, J. Am. Ceram. Soc. 98 (2015) 2796–2802, https://doi.org/10.1111/jace.13681.

[26] R.D. Shannon, Revised effective ionic radii and systematic studies of interatomic distances in halides and chalcogenides, Acta Crystallogr. A. 32 (1976) 751–767, https://doi.org/10.1107/S0567739476001551.

[27] Jiang Dong Tao, Amiya K. Mukherjee, The influence of oxygen vacancy on the optical transmission of an yttria–magnesia nanocomposite, Scripta Mater. 64 (2011) 1095–1097, https://doi.org/10.1016/j.scriptamat.2011.02.029.

[28] Y.R. Luo, Comprehensive Handbook of Chemical Bond Energies, CRC Press, Boca Raton, FL, 2007.

[29] H. Yoshida, S. Hashimoto, T. Yamamoto, Dopant effect on grain boundary diffusivity in polycrystalline alumina, Acta Mater. 53 (2005) 433–440, https://doi.org/10.1016/j.actamat.2004.09.038.

[30] J.B. Gruber, R.P. Leavitt, C.A. Morrison, N.C. Chang, Optical spectra, energy levels, and crystal-field analysis of tripositive rare-earth ions in Y_2O_3. IV. C_{3i} sites, J. Chem. Phys. 82 (1985) 5373–5378, https://doi.org/10.1063/1.448621.

[31] Vijay Singh, Vineet Kumar Rai, Benjamin Voss, Markus Haase, R.P.S. Chakradhar, D. Thirupathi Naidu, Sang Hwan Kim, Photoluminescence study of nanocrystalline Y_2O_3:Ho^{3+} phosphor, Spectrochim. Acta 109 (2013) 206–212, https://doi.org/10.1016/j.saa.2013.01.082.

[32] Feng Qin, Yangdong Zheng, Ying Yu, Zhemin Cheng, Pouran Sadat Tayebi, Wenwu Cao, Zhiguo Zhang, Ultraviolet and violet upconversion luminescence in Ho^{3+}-doped Y_2O_3 ceramic induced by 532-nm CW laser, J. Alloys Compd. 509 (2011) 1115–1118, https://doi.org/10.1016/j.jallcom.2010.09.188.

[33] A. Ciric, S. Stojadinovic, Structural and photoluminescence properties of Y_2O_3 and Y_2O_3:Ln^{3+} (Ln = Eu, Er, Ho) films synthesized by plasma electrolytic oxidation of yttrium substrate, J. Lumin. 217 (2020), 116762, https://doi.org/10.1016/j.jlumin.2019.116762.

[34] T. Biljan, Preparation, characterization and luminescence of nanocrystalline Y_2O_3: Ho, J. Alloys Compd. 431 (2007) 217–220, https://doi.org/10.1016/j.jallcom.2006.05.050.

[35] W.F. Krupke, Induced-emission cross sections in neodymium laser glasses, IEEE J. Quant. Electron. 10 (1974) 450–457, https://doi.org/10.1109/JQE.1974.1068162.

[36] L. Fornasiero, E. Mix, V. Peters, K. Petermann, G. Huber, Czochralski growth and laser parameters of RE^{3+}-doped Y_2O_3 and Sc_2O_3, Ceram. Int. 26 (2000) 589–592, https://doi.org/10.1016/S0272-8842(99)00101-7.

[37] C. Krankel, Rare-earth-doped sesquioxides for diode-pumped high-power lasers in the 1-, 2-, and 3-μm spectral range, IEEE J. Sel. Top. Quant. 21 (2015), 1602013, https://doi.org/10.1109/JSTQE.2014.2346618.

[38] P.J. Dereń, K. Lemański, Cross relaxation in $CaTiO_3$ and $LaAlO_3$ perovskite nanocrystals doped with Ho^{3+} ions, J. Lumin. 154 (2014) 62–67, https://doi.org/10.1016/j.jlumin.2014.04.008.
[39] K.L. Nash, R.C. Dennis, N.J. Ray, J.B. Gruber, D.K. Sardar, Absorption intensities, emission cross sections, and crystal field analysis of selected intermanifold transitions of Ho^{3+} in Ho^{3+}:Y_2O_3 nanocrystals, J. Appl. Phys. 106 (2009), 063117, https://doi.org/10.1063/1.3211298.
[40] D.L. Dexter, A theory of sensitized luminescence in solids, J. Chem. Phys. 21 (1953) 836–850, https://doi.org/10.1063/1.1699044.